STRIPAK complex defects result in pseudosexual reproduction in *Cryptococcus neoformans*

Patricia P. Peterson[1], Sarah Croog[1], Yeseul Choi[1], Sheng Sun[1], and Joseph Heitman[1*]

[1] Department of Molecular Genetics and Microbiology, Duke University Medical Center, Durham, North Carolina, 27710, USA.

* Corresponding author

Email: heitm001@duke.edu (JH)

Keywords: pseudosexual reproduction, PP2A, sexual development, nuclear inheritance, meiosis, phosphatase

Abstract

STRIPAK is an evolutionarily conserved signaling complex that coordinates diverse cellular processes across fungi and animals. In the human fungal pathogen *Cryptococcus neoformans*, STRIPAK was recently shown to play critical roles in maintaining genome stability and controlling both sexual and asexual development. In *Cryptococcus*, sexual reproduction is closely linked to virulence, and our findings demonstrate that the STRIPAK complex plays key roles in both processes. Here, we further investigate the specific roles of the STRIPAK catalytic subunit Pph22 and its regulatory partner Far8 during sexual development. We show that while *pph22*Δ mutants are defective in α-**a** sexual reproduction, exhibiting impaired meiotic progression and a failure to produce viable spores, the deletion of *PPH22* resulted in exclusive pseudosexual reproduction, with progeny inheriting nuclear genomes solely from the wild-type parent. Overexpression of *PPG1*, a related phosphatase, rescued growth and developmental defects in *pph22*Δ mutants, and restored the preference for α-**a** sexual reproduction over pseudosexual reproduction during mating, suggesting functional redundancy within the STRIPAK signaling network. Furthermore, deletion of *FAR8*, another component of the STRIPAK complex, also led to a high rate of pseudosexual reproduction during α-**a** sexual mating, reinforcing the role of STRIPAK in modulating reproductive modes in *C. neoformans*, possibly through regulating nuclear inheritance and meiotic progression. Together, these findings highlight the distinct contributions of STRIPAK to sexual reproduction in *C. neoformans* and suggest that disruptions of this complex affect genome integrity and inheritance mechanisms, with broader implications for fungal adaptation and pathogenesis.

Introduction

In eukaryotic cells, cellular processes are orchestrated by the coordinated activities of protein kinases and phosphatases. Among these, protein phosphatase 2A (PP2A) is a pivotal serine/threonine phosphatase that governs essential functions in cell growth, metabolism, stress responses, proliferation, and differentiation [1-5]. PP2A operates as a heterotrimeric complex, consisting of a scaffold A subunit, a catalytic C subunit, and a regulatory B subunit, which dictates substrate specificity and pathway regulation [6-8]. One key regulatory B subunit is striatin, a core component of the striatin-interacting phosphatase and kinase (STRIPAK) complex, a highly conserved signaling complex that integrates phosphatase and kinase activity to govern developmental and cellular processes across eukaryotes [1, 9-11]. STRIPAK assembly begins with the formation of the PP2A-striatin holoenzyme, which serves as a platform for recruiting additional components to build a larger signaling module [1, 12]. STRIPAK complexes have been identified and characterized in yeasts, filamentous fungi, and mammals, including humans, underscoring their evolutionary conservation. While STRIPAK is broadly conserved across eukaryotes, its functional roles can be context dependent, varying across different organisms and cellular environments [11, 13].

In fungi, STRIPAK is required for both sexual and asexual development, influencing key processes such as cell cycle progression, conidiation, cell fusion, and sporulation [10, 14-17]. In yeasts, STRIPAK-like complexes containing PP2A components are important in the pheromone response pathway and cytokinesis during the sexual cycle [18-20]. In filamentous ascomycetes, STRIPAK homologs have been extensively studied for their roles in sexual and asexual propagation [15, 17, 21-23]. In these species, STRIPAK is essential for the formation of mature fruiting bodies, which are highly complex multicellular structures that arise during sexual reproduction, as well as for asexual growth through conidiation [24, 25]. Similarly, in plant pathogenic fungi such as *Magnaporthe oryzae, Collectrichum graminicola,* and *Fusarium* species, STRIPAK is linked to developmental transitions that enhance virulence, affecting the

48 ability of these pathogens to infect host tissues [26-29]. More recently, STRIPAK has been
49 characterized in the basidiomycete pathogens *Ustilago maydis* and *Cryptococcus neoformans,*
50 where it plays conserved roles in vegetative growth and sexual reproduction [11, 30]. In
51 *Cryptococcus*, STRIPAK also contributes to genome stability, virulence, and pathogenesis,
52 highlighting its broader significance beyond development.

53 *C. neoformans* is a human fungal pathogen in which sexual reproduction has been
54 linked to virulence. Among natural isolates, the α mating type is more prevalent and has been
55 associated with increased virulence, while sexual basidiospores and desiccated yeast cells
56 serve as infectious propagules [31-34]. The dimorphic transition of budding yeast to hyphal
57 growth after mating has also been implicated in pathogenesis, and the formation of sexual
58 structures in environmental niches may enhance fungal survival [35]. Mating between cells of
59 the two opposite mating types, α and **a**, begins with cell-cell fusion, followed by hyphal
60 filamentation, and the formation of a basidium, where nuclear fusion and meiosis occur. After
61 meiosis, nuclei are partitioned into budding spores produced from the basidium, which undergo
62 mitotic division to produce spore chains [36]. Notably, each basidium represents a single meiotic
63 event, and the resulting basidiospores, which form in chains, exhibit distinct adjacent genotypes
64 due to the segregation of alleles during meiosis [37]. This enables the generation of diverse
65 offspring from a single mating event, which may enhance dispersal and dissemination in the
66 environment. Altogether, this sexual cycle contributes not only to genetic diversity but also to
67 environmental persistence and ecological adaptability.

68 In addition to conventional α-**a** sexual reproduction, *Cryptococcus* can undergo
69 pseudosexual reproduction, an alternative reproductive strategy that results in uniparental
70 nuclear inheritance following mating [38]. Unlike classic meiosis, where both parental nuclei
71 contribute genetic material via recombination to produce haploid progeny, pseudosexual
72 reproduction involves the preferential retention of one parental nucleus while the other is lost or

excluded, leading to meiotic progeny whose nuclear genome is genetically identical to one parent and thus lack meiotic recombination. Mitochondrial uniparental inheritance (UPI) also occurs during this process, with mitochondria preferentially inherited from the *MAT***a** parent [39]. This process shares striking similarities with hybridogenesis, a reproductive mode observed in some animals where hybrid offspring selectively eliminate one parental genome during gametogenesis, ensuring uniparental inheritance in subsequent generations [40]. In *Cryptococcus*, pseudosexual reproduction may facilitate progeny survival and expansion in environments where compatible mating partners are scarce, particularly when high genetic divergence or karyotype variation limits traditional mating. Despite its potential role in adaptation and persistence, the molecular mechanisms underlying this process, and the genetic factors involved, remain largely unknown.

In this study, we investigated the roles of Pph22 and Far8, two key components of the STRIPAK complex, which are critical for *C. neoformans* sexual development. Genotyping and whole-genome sequencing of progeny from *pph22*Δ × wild-type crosses revealed that reproduction occurs exclusively through pseudosexual reproduction, with uniparental nuclear inheritance derived solely from the wild-type parent. Fluorescence microscopy further demonstrated that while *pph22*Δ nuclei can migrate into the basidium and initiate meiosis, they fail to generate viable spores, implicating *PPH22* in meiotic progression. Additionally, overexpression of *PPG1*, a functionally related phosphatase, suppressed defects in vegetative growth, stress responses, and sexual growth caused by loss of *PPH22*, highlighting potential compensatory mechanisms within the STRIPAK network. Notably, we found that pseudosexual reproduction also occurs at a high rate in *far8*Δ mutant x wild type crosses, further supporting a role for STRIPAK in coordinating nuclear inheritance and meiotic processes. These findings establish STRIPAK as a key regulatory network in *Cryptococcus* reproduction and suggest that disruptions to this complex may broadly influence genetic stability and inheritance mechanisms in this fungal pathogen.

Results

*pph22*Δ mutants exhibit reduced mating efficiency and abnormal sexual structures

We previously showed that deletion of *PPH22* causes severe mating defects during α-**a** sexual reproduction, as well as in a self-fertile α/**a** diploid strain, leading to significantly delayed sexual development [30]. To further investigate the dynamics of *pph22*Δ mutants during mating, *pph22*Δ strains were crossed with a wild-type partner of the opposite mating type and incubated on MS medium. To overcome the growth defects of *pph22*Δ on nutrient-limited MS media, mating was facilitated by pre-growing mutant cells before adding a smaller amount of wild-type cells, as described previously [30]. After six weeks of incubation, wild-type crosses displayed extensive hyphal growth, basidia formation, and basidiospore production. In contrast, *pph22*Δ x wild type mating patches showed only limited signs of sexual development (Fig 1A). Most patches lacked visible sexual structures, though occasional hyphae and basidia were observed. Basidia were often bald or produced few spores, and many spores appeared collapsed rather than forming the elongated spore chains characteristic of wild-type mating.

To observe morphological differences in sexual structures between *pph22*Δ and wild-type crosses at a higher resolution, scanning electron microscopy (SEM) of the mated strains was performed. In *pph22*Δ x wild type crosses, many basidia terminating from the end of a hyphal branch were considerably rounded and enlarged compared to the wild-type cross and did not produce spores (Fig 1B). When spores were observed, they often had a collapsed appearance, similar to what was seen by light microscopy (Fig 1A). During α-**a** sexual reproduction in the wild type x wild type cross, the clamp cells, which are critical for faithful segregation of nuclei in the dikaryotic hyphae [41, 42], were fused to the subapical cell in the elongating hyphal branch. In mated *pph22*Δ x wild type, both fused and unfused clamp cells could be observed along the same hypha, suggesting a potential defect in nuclear distribution or clamp cell fusion. Due to the observed defects in mating, we quantified cell–cell fusion frequency by incubating crosses between *pph22*Δ*::NAT* and wild type::*NEO* strains on MS

126 medium for three days. After incubation, cells were harvested and plated on YPD supplemented
127 with either NAT, NEO, or both NAT and NEO. Crosses between wild type::*NAT* and wild
128 type::*NEO* strains were included as a control. Fusion events were quantified by counting colony-
129 forming units (CFUs) on YPD+NAT+NEO plates, which represent dual-resistant fusion products.
130 Fusion frequency was calculated as the number of CFUs on YPD+NAT+NEO divided by the
131 sum of CFUs on YPD+NAT and YPD+NEO, representing the total recovered population. A
132 significant reduction in fusion frequency was observed in *pph22*Δ**a** × WTα and *pph22*Δα × WT**a**
133 crosses compared to the wild-type control (Fig S1A). There was a significant reduction in cell-
134 cell fusion frequency in *pph22*Δ**a** x WTα and *pph22*Δα x WT**a** crosses (5.1% to 5.7% of WT x
135 WT). Taken together, these results suggest that *PPH22* is critical for α-**a** sexual mating and
136 proper sexual development.
137

138 **Progeny from *pph22*Δ x wild type crosses are produced exclusively through**
139 **pseudosexual reproduction**

140 To further investigate the reproductive mode of *pph22*Δ x WT crosses, spores were
141 dissected from individual basidia for phenotypic and genotypic analysis. *pph22*Δ mutant strains
142 have severe growth defects and form significantly smaller colonies compared to wild type.
143 Germinated spores from *pph22*Δ x WT formed colonies that were fast growing and uniform in
144 size on YPD (Fig S1B). Streaking onto YPD and YPD+NAT (selecting for the *pph22*Δ*::NAT*
145 mutation) showed that all dissected spores were NAT-sensitive, indicating the absence of
146 *pph22*Δ mutants among the recovered progeny, potentially suggesting that the spores originated
147 from unisexual reproduction of the wild-type parental strain [43]. To investigate this possibility,
148 spores were dissected from basidia of two independent *pph22*Δ**a** × WTα crosses and one
149 *pph22*Δα × WT**a** cross to yield viable progeny. PCR genotyping of the *STE20* gene in the
150 mating-type locus *(MAT*) revealed that all progeny from each individual basidium contained
151 either the *MAT***a** or the *MAT*α allele, which strictly corresponded to the allele from the wild-type

152 parent (Table 1, Fig S1C). PCR of the *COX1* gene also indicated that the mitochondria was
153 predominantly inherited from the *MAT***a** parent, consistent with mitochondrial uniparental
154 inheritance (mito-UPI) in *Cryptococcus* [39, 44]. *MAT*α mitochondrial inheritance was observed
155 in *pph22*Δ**a** × WTα crosses at a frequency of 32% (7 out of 22 basidia), which is higher than the
156 expected frequency of *MAT*α mitochondria leakage of around 5% to 10% [45]. However, six of
157 these basidia originated from the same mating spot, leaving open the possibility that the
158 inherited *MAT*α mitochondria in the progeny resulted from a single mating event. Similarly, in
159 random spore dissection, 15 out of 65 germinated progeny possessed *MAT*α mitochondria, but
160 were dissected from a single mating spot. It is unclear whether the *pph22*Δ mutation leads to
161 increased *MAT*α mitochondrial inheritance. These results suggest that progeny from *pph22*Δ ×
162 WT inherited only the wild-type parental nuclei. Additionally, the presence of mitochondria from
163 the *MAT***a** parent in *MAT*α progeny indicates that these progeny are not the result of unisexual
164 reproduction. These observations demonstrate that the mode of reproduction in *pph22*Δ × WT
165 crosses is pseudosexual, during which cells of the opposite mating type fuse but the nuclear
166 content of only one parental nucleus is transmitted to the progeny [38].
167 Following PCR genotyping assays, whole-genome sequence analysis was conducted to
168 determine if there was any evidence of meiotic recombination in the F1 progeny from *pph22*Δ**a**
169 × WTα. The *pph22*Δ strains utilized in this study were obtained from dissection of a KN99**a**/α
170 *PPH22/pph22*Δ heterozygous diploid mutant and are congenic with H99 [30, 46]. Besides the
171 mating-type locus on chromosome 5, there are two other genomic regions on chromosomes 11
172 and 14 that differ between H99α and KN99**a** background strains [47, 48]. Twelve progeny from a
173 single basidia (Table 1, spot D basidium 1) were subjected to Illumina whole-genome
174 sequencing and reads were aligned to the H99α reference genome for variant calling and SNP
175 analysis (Fig 2). The KN99**a** *pph22*Δ parental strain and the KN99**a**/α diploid strain (CnLC6693)
176 from which it was derived served as controls. Variant analysis confirmed that only the H99α
177 nuclear genome was inherited in the progeny, as evidenced by the absence of SNPs at the

178 indicated polymorphic loci. Alignment of reads from the KN99 parental strains and progeny to
179 the H99α mitochondrial genome also confirmed the presence of the intron in the KN99**a** *COX1*
180 gene, supporting the results from PCR genotyping. Collectively, the lack of meiotic
181 recombination supports that the progeny from mating of *pph22*Δ × WT arose through a
182 pseudosexual reproductive process and not via α-**a** sexual reproduction.
183

184 **Uniparental nuclear inheritance observed after mating via fluorescence microscopy**

185 Previous studies with fluorescently marked nuclei provided evidence that pseudosexual
186 reproduction in *Cryptococcus* results from loss of one parental nucleus during hyphal branching
187 following mating [38]. A similar approach was taken to investigate nuclear migration during
188 mating in *pph22*Δ × WT crosses. The gene encoding the nucleolar protein Nop1 was fused with
189 GFP or RFP (mCherry) and introduced ectopically into the safe haven region of *pph22*Δ**a**
190 (*NOP1-GFP-NEO)*, KN99**a** (*NOP1-GFP-NEO)*, and H99α (*NOP1-mCherry-HYG*) [49].
191 Homologous recombination at the target locus was confirmed by PCR genotyping. *pph22*Δ and
192 KN99**a** strains expressing Nop1-GFP were crossed with H99α expressing Nop1-RFP on MS
193 media and monitored for signs of mating (Fig S2A). In wild-type crosses, live-cell imaging
194 revealed hyphae containing both GFP- and RFP-tagged proteins following cell-cell fusion,
195 maintaining a stable dikaryotic state throughout hyphal elongation and branching, with green
196 and red fluorescent signals overlapping or appearing in close proximity (Fig S2B). In the basidial
197 heads, the final stages of the sexual cycle were observed, including karyogamy, where the two
198 parental nuclei fused, followed by meiosis and subsequent inheritance of fluorescent tags from
199 both parents in the haploid basidiospores. In total, 27 basidia from two independent crosses
200 were observed to produce spores that contained both fluorescent markers.

201 Nuclear dynamics in *pph22*Δ crosses were notably distinct from those in wild-type
202 crosses. As expected, *pph22*Δ**a** x H99α exhibited decreased mating efficiency, but spore
203 production was still observed after six to eight weeks of incubation (Fig S2A). Fluorescence

204 imaging showed that both red and green nuclear markers initially coexisted within the same
205 hyphal compartment and could be tracked along the elongating hyphal branch. However, at
206 certain branch points, the green *pph22*Δ nucleus was selectively lost, allowing only the red wild-
207 type nucleus to undergo meiosis in the terminating basidium (Fig S2C). Among 40 basidia
208 analyzed from four independent crosses, 15 did not produce spores. Of these, 12 displayed
209 both red and green signals in the basidium head, while the remaining three showed only the red
210 signal. The other 25 basidia successfully produced spores, with 20 containing only the signal
211 from the wild-type parent. This finding aligns with previous work suggesting that hyphal
212 branching may facilitate nuclear exclusion, which can be followed by endoreplication and
213 meiosis of the retained nucleus [38].

214 In contrast, there were also cases in crosses of *pph22*Δ x WT where the wild-type
215 nucleus was lost following hyphal branching, after which the resulting sexual structures
216 exhibited abnormal morphology (Fig 3). Several observations suggested that, after the loss of
217 the red wild-type signal in a hyphal branch, the green *pph22Δ* nucleus could undergo
218 endoreplication followed by nuclear division, resulting in two green nuclei within a single hyphal
219 compartment, indicating a mechanism by which a dikaryotic-like state could be reestablished
220 (Figure 3A). There were also instances where, following wild-type nuclear exclusion, only the
221 *pph22*Δ fluorescent signal was inherited in the basidiospores, which appeared collapsed onto
222 the basidium head (Fig 3B, 3C). Notably, five basidia that produced spores exhibited only the
223 green signal in the progeny., suggesting that the *pph22*Δ mutant nucleus is capable of migrating
224 into the basidium, undergoing diploidization, and potentially entering the meiotic process.
225 However, despite this apparent progression, the consistent inability to recover *pph22*Δ mutant
226 progeny from any dissection of *pph22*Δ x WT crosses, indicates a meiotic or post-meiotic defect
227 that prevents successful germination. There was also evidence that maintenance of only the
228 *pph22*Δ nucleus negatively impacted hyphal morphology, significantly altering both the shape

229 and structure (Fig 3D). Additionally, in another hyphal branch, there were two nuclei detected for
230 each color to yield four nuclei in individual cells, suggesting a failure in nuclear sorting or
231 segregation following DNA replication. Together with spore genotyping analyses, these findings
232 suggest that: 1) pseudosexual reproduction may occur through the loss of one parental nucleus
233 during hyphal branching and 2) the *pph22*Δ mutation disrupts normal sexual development,
234 including nuclear migration, hyphal morphology, and sporulation.
235
236 **α-a sexual reproduction is restored in *pph22*Δ *suppressor* mutants**
237 *pph22*Δ strains can accumulate spontaneous suppressor mutations that restore mating,
238 hyphal growth, basidia production, and sporulation nearly to the wild-type level (Fig 4A) [30]. To
239 determine if the *pph22*Δ *suppressor* (*sup)* mutant strains could also suppress pseudosexual
240 reproduction, F1 progeny from *pph22*Δ *sup* x WT crosses were analyzed. In one such cross,
241 germinated spores containing the *NAT* drug-resistance marker were recovered during
242 dissection, in contrast to strictly NAT-sensitive *pph22*Δ x WT progeny, providing evidence the
243 suppressor mutation could restore *pph22*Δ spore viability following α-**a** sexual mating, although
244 the resulting colonies were notably smaller in size (Fig 4B). The frequency of *pph22*Δ::*NAT*
245 among the progeny was 45%, consistent with the expected segregation of a single selectable
246 allele. However, in crosses with two other independently derived *pph22*Δ *sup* strains, no NAT
247 resistant progeny were recovered, suggesting incomplete suppression of *pph22*Δ mutant
248 defects following mating in those strains.
249 We next investigated mating type and mitochondrial genome segregation in *pph22*Δ *sup*
250 x WT crosses. All *pph22*Δ *sup* isolates that were obtained in our previous study possess the
251 *MAT*α allele and therefore were crossed with KN99**a**. This led to a complication in using the
252 same PCR genotyping strategy to determine how the mitochondria was inherited in the progeny
253 from these crosses, as KN99**a** and KN99α background strains have identical mitochondria
254 genomes. Therefore, *pph22*Δ *sup* strains were crossed with the KN99**a** strain SSH118, which

255 carries a recombinant mitochondrial genome, and restriction fragment length polymorphism
256 (RFLP) analysis was used to identify the parental source of the mitochondrial genome in the
257 progeny (Fig 4C, S3). In each *pph22*Δ *sup* x WT cross, each basidium that was dissected came
258 from different mating spots, so that the progeny analyzed were the result of independent mating
259 events. The *MAT* allele was determined through PCR genotyping of the *STE20* gene, as in
260 previous experiments, and mitochondrial type was identified through PCR amplification of *COX1*
261 followed by BsrI digestion and RFLP analysis (Fig S3B, S3C, S3D). Both **a** and α mating types
262 were found among the genotyped basidia and, interestingly, many progeny were heterozygous
263 for the *MAT* allele (Fig 4C, S3E). The fact that progeny exhibiting *MAT* heterozygosity also came
264 from basidia with high germination rates suggests that this cannot be explained by aneuploidy
265 alone, as an imbalance in chromosome number in aneuploid spores would lead to reduced
266 germination rates.

267 Flow cytometry analysis of progeny heterozygous for the *MAT* locus revealed that
268 increased DNA content correlated with the presence of the *pph22*Δ*::NAT* deletion allele (Fig
269 S3F). Specifically, NAT-sensitive progeny remained haploid, while all NAT-resistant progeny
270 displayed peaks at 1N, 2N, and 4N, suggesting altered DNA replication or disrupted ploidy
271 regulation in these cells. These results suggest that *PPH22* may have a role in ploidy regulation,
272 and its loss may disrupt cell cycle regulation and lead to altered DNA inheritance patterns.
273 Further analysis, such as whole-genome sequencing, could help clarify which process may be
274 maintaining *MAT* heterozygosity in the NAT-sensitive progeny. While mitochondria in the
275 majority of progeny were inherited from the *MAT***a** parent, progeny from two out of seven basidia
276 from independent mating spots in one of the *pph22*Δ *sup* x WT crosses inherited mitochondria
277 from the *MAT*α parent (Fig S3E). Together, with the genotyping results from *pph22*Δ x WT
278 crosses, these findings suggest that deletion of *PPH22* may also influence mitochondrial
279 inheritance. Although no evidence of pseudosexual reproduction was found in the *pph22*Δ *sup*

280 crosses, the observed α-**a** sexual reproduction was atypical, characterized by an unexpected
281 segregation of mating-type alleles.
282
283 **Overexpression of *PPG1* suppresses loss of *PPH22***
284 All independently obtained *pph22*Δ *sup* mutant strains were found to be aneuploid for a
285 segment of chromosome 6 encompassing seven genes [30]. Of these genes, *PPG1*, which
286 encodes a putative PP2A catalytic subunit and shares significant sequence similarity with
287 Pph22, was overexpressed 40-fold in the *pph22*Δ *sup* mutants compared to wild type [30]. To
288 determine if *PPG1* overexpression was the causative mutation suppressing *pph22*Δ
289 phenotypes, a *PPG1* allele with a constitutively active promoter (P_{TEF1}-*PPG1-NEO)* was
290 integrated into the safe haven 1 of the *PPH22/pph22*Δ heterozygous mutant diploid strain and
291 homologous recombination was confirmed through PCR genotyping. Following self-
292 filamentation on MS media, random spores were dissected and germinated on YPD (Fig 5A).
293 Colonies containing both *NAT* and *NEO* drug resistance markers, confirmed by growth on
294 selective media and PCR genotyping, were faster growing and larger in size than *pph22*Δ
295 mutant colonies, suggesting that overexpression of *PPG1* can partially rescue growth defects of
296 *pph22*Δ.
297 Next, to examine the role of *PPG1* overexpression in response to different nutrient and
298 stress conditions, *pph22*Δ *PPG1-OE*, *pph22*Δ, *pph22*Δ *sup, ppg1*Δ*,* and wild type strains were
299 serially diluted and spotted onto YPD at 25ºC, 30ºC, and 37ºC; YPD with 1 M sorbitol; YPD with
300 rapamycin; and YPD with the immunosuppressive drugs FK506 or cyclosporine A (CsA) (Fig
301 5B). *pph22*Δ exhibited severe growth defects or no growth on YPD at 25ºC, 30ºC, and 37ºC, as
302 well as on YPD supplemented with sorbitol, FK506, or cyclosporine A, which was partially
303 reversed in the *pph22*Δ *sup* strain, consistent with previously published results. On YPD
304 supplemented with rapamycin, on which *pph22*Δ strains do not have noticeable defects
305 compared to wild type, both *pph22*Δ *sup* and *pph22*Δ *PPG1-OE* strains displayed significant

306 growth advantages. Collectively, overexpression of *PPG1* in the *pph22*Δ mutant was able to fully
307 restore or nearly restore growth to wild-type levels under each condition tested, suggesting that
308 P_{TEF1}-*PPG1* is more effective at compensating for *pph22*Δ than overexpression of *PPG1* due to
309 aneuploidy in *pph22*Δ *sup* strains.

310 It was surprising that *ppg1*Δ did not phenocopy *pph22*Δ, and only exhibited growth
311 defects on YPD at 25ºC and on YPD supplemented with sorbitol or rapamycin, compared to
312 growth on YPD at 30ºC. In fact, *ppg1*Δ displayed similar growth to *pph22*Δ *PPG1-OE* under
313 several conditions, including growth at 30ºC and 37ºC as well as in the presence of FK506 and
314 CsA. These results suggest that while Pph22 and Ppg1 are hypothesized to have similar
315 functions and may play partially compensatory roles, Pph22 is likely the primary catalytic
316 subunit of PP2A, as its loss leads to more severe effects than the loss of *PPG1.* To assess the
317 abilities of *ppg1*Δ and *pph22*Δ *PPG1-OE* strains to produce melanin pigment and
318 polysaccharide capsule, important virulence factors to protect cells from the host immune
319 response during *Cryptococcus* infection. To induce melanin and capsule production, cells were
320 grown on Niger seed agar and in RPMI media, respectively, with both incubated at 30ºC.
321 *pph22*Δ *sup* and *pph22*Δ *PPG1-OE* produced similar amounts of melanin and were comparable
322 to the wild type, while *ppg1*Δ could not produce melanin, similar to the *lac1*Δ negative control
323 (Fig 5C). These results suggest that *PPG1* is required for melanin production, while *PPG1*
324 overexpression in the *pph22*Δ background is sufficient to restore this virulence trait. India ink
325 counterstaining of RPMI-grown cells showed that *PPG1* overexpression restored normal cell
326 morphology in the *pph22*Δ mutant, though capsule production was still impaired (Fig 5D). In
327 contrast, *ppg1*Δ cells could produce capsule, albeit to a lesser extent than wild-type cells.
328 Together, these findings are consistent with the idea that *PPG1* can functionally compensate for
329 the loss of *PPH22* in certain contexts.

330 To further explore the functional differences between Pph22 and Ppg1, 3D structural
331 models of the STRIPAK complex with either Pph22 or Ppg1 as the catalytic subunit were
332 generated with AlphaFold3 [50]. The resulting Pph22-containing structure was comparable to
333 the previously published model generated with AlphaFold2, though slight differences in folding
334 were observed [30, 51]. The two models appeared largely similar, indicating that Ppg1 can
335 potentially assemble into a complex with the other STRIPAK subunits (Fig S4A, S4B). Cryo-EM
336 studies of the human STRIPAK complex have demonstrated that Far8 forms a homotetramer,
337 serving as a scaffold at the base of the complex [12]. To assess whether *Cryptococcus* Far8
338 could similarly assemble into a tetramer, a structural model was generated using four copies of
339 the Far8 protein (Fig S4C). This model was then combined with either the Pph22-Tpd3 or Ppg1-
340 Tpd3 heterodimers to examine PP2A assembly. Both models appeared highly similar overall,
341 though the four Far8 proteins adopted slightly different conformations in each structure (Fig
342 S4D, S4E). These findings suggest that both Pph22 and Ppg1 can potentially integrate into
343 STRIPAK in a comparable manner, perhaps filling analogous roles within the complex.

344 Finally, the involvement of Ppg1 during mating was examined by crossing *ppg1*Δ and
345 *pph22*Δ *PPG1-OE* strains with wild type. Similar to what has been observed in *pph22*Δ crosses,
346 *ppg1*Δ x WT exhibited delayed mating and hyphae were produced only in isolated spots on the
347 mating patch after six weeks of incubation (Fig 5E compared to Fig 1A). With further incubation,
348 more extended hyphal branches were produced but mostly bald basidia heads with almost no
349 spore formation. In contrast, *pph22*Δ *PPG1-OE* x WT crosses displayed signs of mating at a
350 similar rate to wild type and produced abundant basidia with spore chains (Fig 5E compared to
351 Fig 4A). These findings indicate that Ppg1 plays a crucial role during mating and sexual
352 development, similar to Pph22. Taken together, this further supports the conclusion that *PPG1*
353 overexpression is the key mutation suppressing *pph22*Δ, as targeted overexpression of *PPG1* in
354 the *pph22*Δ background similarly restored both mating and growth deficiencies.

355

356 **Pseudosexual reproduction also occurs at a high rate in *far8*Δ mutant crosses**

357 It has been reported that pseudosexual reproduction occurs at a rate of ~1% between
358 wild-type mating partners with compatible parental genomes, as well as in partners with
359 incompatible parental genomes due to genetic divergence or genome structure variation [38,
360 52]. The analyses presented here demonstrated that deletion of *PPH22* results in exclusively
361 pseudosexual reproduction following α-**a** sexual mating. To further investigate whether other
362 mutations in the STRIPAK complex influence pseudosexual reproduction, *far8*Δ mutant crosses
363 were analyzed. Far8 has also been shown to be critical during *Cryptococcus* sexual
364 development, with *far8*Δ strains exhibiting severe defects in hyphal production and sporulation.
365 To inspect the sexual structures of *far8*Δ x WT crosses in higher resolution, hyphae, basidia,
366 and spore chains were imaged with SEM (Fig 6A). Spores were observed budding from the
367 basidia in irregular numbers, often exceeding the typical set of four. In some cases, seven or
368 more spores emerged independently from separate sites on a single basidium. *far8*Δ strains
369 have been predominantly identified as diploid, suggesting that mating could result in triploid
370 meiosis. This raises the possibility that the observed irregular spore structures may be
371 influenced by the unique genomic composition in the basidium.

372 Next, spores were dissected from individual basidia from both *far8*Δ **a** x WTα and *far8*Δ
373 α x WT**a** crosses. Spores that germinated formed mostly homogenously sized colonies on YPD
374 and did not contain the drug resistance marker, but occasionally small, slow-growing *far8*Δ
375 mutant colonies were obtained (Fig 6B). In total, spores from 16 basidia obtained from nine
376 independent mating spots were dissected and genotyped (Fig 6C). Given the genomic instability
377 of triploid meiosis, reduced spore viability was expected. However, surprisingly, 10 out of 16
378 basidia exhibited germination rates above 70%, with an overall average of 79%, which is
379 comparable to the germination rate observed in progeny from wild-type crosses. PCR
380 genotyping of the *MAT* locus and mitochondrial DNA in progeny from 11 out of 16 dissected

basidia were consistent with pseudosexual reproduction, characterized by uniparental nuclear inheritance from only the wild-type parent, a pattern also observed in *pph22*Δ mutant crosses, and mitochondrial inheritance from the *MAT***a** parent. Heterozygosity at the *MAT* locus was also detected in some progeny from the remaining five basidia of the *far8*Δ x WT crosses, resembling the findings in the *pph22*Δ *sup* x WT crosses. Notably, 11 out of 16 progeny possessing both *MAT***a** and *MAT*α also had the *far8*Δ mutant allele, which may be attributed to the altered genomic structure of the *far8*Δ parental strains. Taken together, these results suggest that loss of STRIPAK components *PPH22* or *FAR8* drives pseudosexual reproduction, with the mutant nuclei at a selective disadvantage to the wild-type nucleus, as shown by uniparental nuclear inheritance predominantly from the wild-type parent (Fig S5).

391 **Discussion**

392 The STRIPAK complex has been broadly recognized across fungi as a critical regulator
393 of both asexual and sexual development. In *C. neoformans*, we previously demonstrated that
394 mutants defective in STRIPAK components exhibit defects in several developmental processes,
395 along with increased genome instability, leading to segmental and whole-chromosome
396 duplications or losses [30]. Additionally, STRIPAK mutations were shown to impact the
397 production of virulence traits and pathogenesis during infection. In this study, we further
398 explored the specific roles of STRIPAK during mating and sexual development, identifying two
399 genes, *PPH22* and *FAR8*, that were directly involved in pseudosexual reproduction. This
400 unusual reproductive strategy, which was previously characterized in our lab, occurs when there
401 is incompatibility between mating partners due to genetic divergence or genome structure
402 variation, allowing *C. neoformans* to overcome reproductive barriers [38]. While previously
403 predicted to occur at low frequencies, pseudosexual reproduction enables the production of
404 viable offspring in conditions where successful α-**a** sexual reproduction is not possible or is
405 inefficient, contributing to survival and adaptation.

406 It has been hypothesized that pseudosexual reproduction may preferentially favor the
407 predominance of one mating type over the other and that specific factors influence which
408 nucleus is selectively lost following mating. Our findings provide evidence for genetic factors
409 influencing pseudosexual reproduction, as progeny from crosses involving *pph22*Δ or *far8*Δ
410 mutants exclusively inherited their nuclear genome from the wild-type parent. This supports the
411 hypothesis that, even in cases where mating partners are genetically compatible, intrinsic gene
412 variation can endow one genome with a selective advantage over the other. Such selective
413 inheritance could potentially contribute to fungal adaptation, as it might allow for the retention of
414 beneficial genetic traits while discarding less advantageous ones. Given that loss of *PPH22* or
415 *FAR8* leads to widespread genome instability, including segmental and whole chromosomal
416 aneuploidy, it is likely that these defects impose a fitness cost during sexual development,

417 favoring the retention of the more stable wild-type genome. The defective spore formation
418 observed in *pph22*Δ and *far8*Δ mutants, along with the presence of aberrant DNA content in the
419 progeny, suggests that these mutations may impair proper chromosome segregation or meiotic
420 progression. As a result, selective nuclear retention in pseudosexual reproduction may serve as
421 a mechanism to safeguard genomic integrity, ensuring that only nuclei with fewer deleterious
422 mutations or with more favorable genomic configurations contribute to the next generation.

423 During *Cryptococcus* sexual development, the process of nuclear migration, segregation
424 of nuclei within dikaryotic hyphae, and meiosis are tightly coordinated processes that ensure
425 proper exchange and inheritance of genetic material [34, 53]. STRIPAK has been implicated in
426 actin cytoskeletal organization in other organisms, raising the possibility that its components
427 may play a role in regulating nuclear dynamics during mating [18, 54-57]. In *Cryptococcus*,
428 sexual reproduction involves an extended dikaryotic phase prior to karyogamy, requiring precise
429 nuclear positioning within hyphae. Our fluorescence microscopy data indicate that *pph22*Δ
430 mutants exhibit nuclear segregation defects, as their nuclei frequently fail to reach the basidium.
431 This suggests that *PPH22* may be required for proper nuclear migration during hyphal
432 branching and elongation. However, the observation that wild-type nuclei were sometimes lost
433 without generating viable *pph22*Δ spores suggests that *PPH22* also plays a direct role in
434 meiosis. These findings highlight the role of STRIPAK components in maintaining nuclear
435 integrity throughout sexual development.

436 Interestingly, although recessive mutations are typically complemented in a dikaryon by
437 the presence of a wild-type allele in the opposing nucleus, these findings provide additional
438 evidence that *pph22* mutations are haploinsufficient in this context. Developmental defects were
439 observed in dikarya formed between *pph22*Δ and wild-type strains, and importantly, it was
440 previously demonstrated that a *PPH22/pph22*Δ heterozygous diploid is haploinsufficient,
441 supporting the conclusion that a single copy of *PPH22* is insufficient to support normal

442 development in a diploid or dikaryon. This dosage sensitivity may in part explain the dominance
443 of the wild-type genome in pseudosexual reproduction. Additionally, frequent aneuploidy
444 observed in the *pph22*Δ mutant strains may further compromise nuclear division and migration
445 or meiotic progression, contributing to the nuclear selection bias. Together, these data suggest
446 that both haploinsufficiency and genomic instability may underlie the strong inheritance bias and
447 disrupted sexual development seen in *pph22*Δ crosses, potentially serving as a mechanism to
448 eliminate defective nuclei and maintain genome integrity.

449 The relationship between *PPH22* and *PPG1* suggests functional redundancy, as
450 overexpression of *PPG1* can compensate for *pph22*Δ during both vegetative growth and sexual
451 development. This compensation indicates that *PPG1* can partially fulfill the role of *PPH22* in
452 regulating key cellular processes, likely due to their structural and functional similarities.
453 However, despite this redundancy, *PPH22* appears to have a more critical role, as *ppg1*Δ
454 mutants exhibited more subtle phenotypes compared to the severe defects observed in *pph22*Δ.
455 Notably, while deletion of *PPH22* is synthetically lethal with calcineurin inhibition by FK506 or
456 cyclosporine A, deletion of *PPG1* did not cause a significant growth defect under these
457 conditions. This suggests that *PPH22* plays a predominant role in maintaining essential
458 phosphatase activity that becomes indispensable when calcineurin is inhibited, whereas *PPG1*
459 may function as a secondary phosphatase with limited capacity to support survival under these
460 stresses. These findings reinforce the idea that *PPH22* is the primary catalytic subunit of PP2A,
461 with *PPG1* providing only partial redundancy. This difference in phenotypic severity highlights
462 the distinct regulatory contributions of these phosphatases, with *PPH22* playing a dominant role
463 in STRIPAK-dependent processes.

464 Overall, our findings highlight the critical role of the STRIPAK complex in coordinating
465 key aspects of *Cryptococcus* sexual reproduction and development, including nuclear dynamics
466 during mating, genome stability, and meiotic progression. While STRIPAK has been implicated

467 in developmental processes across diverse fungal species, its role in pseudosexual
468 reproduction is intriguing and unique to *Cryptococcus,* where it seems to bear a resemblance to
469 hybridogenesis observed in some animal species. The ability to selectively retain one parental
470 nucleus during mating may serve as a mechanism to maintain genome integrity in the face of
471 genetic instability, ensuring the production of viable progeny when conventional mating
472 pathways are disrupted. Our study provides new insights into the genetic factors that govern
473 sexual reproduction in *Cryptococcus*, shedding light on how STRIPAK complex mutations
474 influence nuclear selection and inheritance. Future studies will explore how STRIPAK
475 coordinates with other signaling pathways, such as calcineurin and MAPK regulation, to direct
476 cellular growth processes. Additionally, investigating whether similar mechanisms operate in
477 other fungal pathogens could reveal broader implications for genome evolution and adaptation.

478 **Materials and methods**

479 **Strains, media, and growth conditions**

480 Strains characterized in this study are listed in Table S1. Strains were prepared for long-
481 term storage as 20% glycerol stocks at -80°C. Fresh cultures were revived and maintained on
482 YPD (1% yeast extract, 2% Bacto Peptone, 2% dextrose) agar medium, incubated at 30°C.
483 *Cryptococcus* transformants harboring dominant drug-resistance markers were selected on
484 YPD medium supplemented with 100 µg/mL nourseothricin (NAT), 200 µg/mL neomycin (G418),
485 or 100 µg/mL hygromycin B (HYG). Strains were grown in YPD liquid cultures at 30°C as
486 indicated. For plate growth assays, strains were cultivated on YPD, Murashige and Skoog (MS)
487 (Sigma-Aldrich M5519), or Niger seed (7% Niger seed, 0.1% dextrose). Sorbitol was added to
488 YPD medium at a 1 M concentration. To analyze cell growth in response to immunosuppressive
489 agents, rapamycin (100 ng/mL), FK506 (1 µg/mL), and cyclosporine A (100 µg/mL) were added
490 to YPD medium. For serial dilution assays, fresh cells were diluted to a starting OD_{600} of 0.1,
491 serially diluted 5-fold, and spotted onto plates for the indicated media and temperature
492 conditions. Plates were incubated for two to seven days and photographed daily. For capsule
493 analysis, strains were incubated for 3 days in RPMI media at 30˚C, followed by negative
494 staining with India ink. For mating assays, strains were incubated on MS plates, face up, in the
495 dark at room temperature for up to eight weeks. Spores dissected from MS plates were
496 germinated on YPD at 30°C for five days.

497

498 **Strain construction**

499 Mutant strains analyzed in this study were generated in the *C. neoformans* H99α,
500 YL99**a,** or KN99**a**/KN99α backgrounds. All genetic manipulations were done using CRISPR-
501 Cas9-mediated mutagenesis and the TRACE system, according to previously published
502 protocols [58, 59]. In brief, Cas9 was amplified from the pBHM2403 plasmid and gRNAs were
503 generated with sequence specific-primers and amplification of the gRNA scaffold from the

504 pBHM2329 plasmid [59]. Donor DNA templates for transformations were generated by PCR or
505 plasmid digestion and purified with the QIAquick gel extraction kit (Qiagen #28704). Cells and
506 DNA were prepared for transformation as described in the TRACE system, and electroporated
507 utilizing a BioRad gene pulser (0.45 kV, 125 μF, 600 Ω). Cells were recovered in YPD media for
508 2-3 hours at 30ºC following electroporation.

509 To generate the *PPG1* overexpression allele, the *TEF1* promoter (1.2 kb) and *PPG1*
510 coding regions were amplified from H99α genomic DNA and assembled into plasmid pSDMA57,
511 digested with XhoI and SpeI, via Gibson assembly (New England Biolabs E5510S) for targeting
512 to the safe haven (SH) locus [49]. GFP tagging of Nop1 was also performed through integration
513 at the safe haven. To facilitate homologous recombination at the target locus, the safe haven
514 plasmid pYSCE5 (pSH-P_{H3}-GFP-HYG) was designed to include a safe haven genomic
515 sequence containing AscI and PacI restriction sites for linearization, along with the histone H3
516 promoter, GFP, and the hygromycin B resistance gene (HYG). The *NOP1* gene, amplified from
517 H99α genomic DNA without its stop codon, was incorporated into plasmid pYSCE5 between the
518 *H3* promoter and GFP, generating pYSCE8 (pSH-H3-NOP1-GFP-HYG). Plasmids for targeted
519 integration at the safe haven were linearized via overnight digestion with AscI and PacI and gel-
520 purified prior to transformation. The *ppg1::NEO* deletion allele was made via PCR amplification
521 of approximately 1 kb homologous 5' and 3' flanking regions to the *PPG1* open reading frame,
522 which were then assembled with the neomycin resistance gene expression cassette (NEO)
523 through overlap PCR [60, 61]. Transformants were plated onto selective media (YPD+NEO or
524 YPD+HYG) and allowed to grow up to 7 days at 30ºC. Stable genomic integrants were verified
525 by diagnostic PCR amplifying the 5′ and 3′ flanking junctions of the insertion site.

526

527 **Primers, PCR genotyping, and RFLP analysis**

528 Primers employed in this study are listed in Table S2. Genomic DNA from strains
529 generated in this study was extracted from cells with the MasterPure Yeast DNA Purification Kit

530 (LGC Biosearch Technologies). Dissected progeny from mated crosses were genotyped by
531 colony PCR. Single colonies were picked into 0.25% SDS and 1 mM EDTA, briefly frozen at -
532 20 °C, and then heated at 100ºC for 10 minutes in a thermocycler. The resulting supernatants
533 were used as DNA templates for PCR. To determine the mating type of *C. neoformans* strains,
534 the *STE20* gene in the *MAT* locus was amplified using primers specific to the *STE20*α and
535 *STE20***a** alleles. The mitochondrial *COX1* gene, which differs in size in KN99 background strains
536 compared to H99 due to the presence of an intron, was probed to determine mitochondrial
537 inheritance. For KN99α *pph22*Δ *sup* crosses, the KN99**a** SSH118 strain, which has a
538 recombinant mitochondrial genome, was used as the wild-type parent to differentiate between
539 mitochondrial genotypes in the KN99 background progeny. After PCR amplification of *COX1*,
540 the resulting PCR product was digested with restriction enzyme BsrI for restriction fragment
541 length polymorphism (RFLP) analysis. Digestion of the *COX1* PCR product amplified from
542 KN99**a**, which contains three BsrI recognition sites, and SSH118, which has two BsrI sites, were
543 used as controls to determine the mitochondrial inheritance of the progeny from *pph22*Δ *sup* x
544 SSH118 crosses.
545
546 **Microscopy**
547 For sample preparation for scanning electron microscopy from mated strains of
548 *Cryptococcus*, an agar slice of the plated cells was fixed in a solution of 4% formaldehyde and
549 4% glutaraldehyde for 2 hours at 4°C. The fixed cells were then gradually dehydrated in a
550 graded ethanol series (30%, 50%, 70%, and 95%), with a 15-minute incubation at 4°C for each
551 concentration. This was followed by three washes with 100% ethanol, each for 15 minutes at
552 4°C. The samples were further dehydrated using a Ladd CPD3 Critical Point Dryer and coated
553 with a layer of gold using a Denton Desk V Sputter Coater (Denton Vacuum, USA). Hyphae,
554 basidia, and basidiospores were observed with a scanning electron microscope with an EDS
555 detector (Apreo S, ThermoFisher, USA). Brightfield, differential interference contrast (DIC), and

556 fluorescence microscopy images were visualized with an AxioScop 2 fluorescence microscope
557 and captured with an AxioCam MRm digital camera (Zeiss, Germany). Consistent exposure
558 times were used for all images captured from the same experiment. Image processing and
559 merging channels of fluorescent images was performed with ImageJ/Fiji software.
560
561 **Cell-cell fusion and mating assays**
562 To induce mating, the indicated strains were grown overnight in YPD medium, diluted to
563 an OD_{600} of 1.0, and 4 µL of each cell suspension was spotted onto MS agar plates. The plates
564 were incubated at room temperature in the dark and monitored for signs of filamentation and
565 sporulation for up to eight weeks. For wild-type mating crosses, *MAT***a** cells (KN99**a**) were mixed
566 with *MAT*α cells (H99α) in equal amounts and spotted onto MS plates. For crosses involving
567 *pph22*Δ and *far8*Δ strains, the following modifications were made to compensate for the
568 impaired growth of these mutants on MS medium. Fresh *pph22*Δ and *far8*Δ mutant cells were
569 first spotted onto MS agar and pre-incubated in the dark at room temperature for two days,
570 without the wild-type mating partner. After pre-growth, wild-type cells of the opposite mating type
571 were added directly on top of the mutant cells at a ten-fold lower cell amount. Twelve mating
572 spots were prepared per plate, with each spotted treated as an independent replicate. A wild-
573 type H99α x KN99**a** cross was included on each plate as a control. Basidiospores were
574 dissected from individual basidia, or randomly dissected, and incubated on YPD medium at
575 30ºC for 3 to 4 days to determine spore viability and germination rates.
576 To assess cell-cell fusion frequency in wild type x *pph22*Δ crosses, KN99**a** or KN99α
577 strains carrying a NEO resistance marker (JOHE10493, JOHE18842) were mixed in 1:10
578 proportions with *pph22*Δ*:NAT* **a** or α strains, spotted onto MS agar, and incubated in the dark at
579 room temperature for 3 days. A KN99**a***::NAT* (JOHE18853) x KN99α*::NEO* (JOHE18842) wild-
580 type cross was used as a control. The entire patch of cells was harvested and serially diluted in
581 PBS before plating onto YPD+NAT, YPD+NEO, and YPD+NAT+NEO selective media. Colony-

582 forming units (CFUs) were counted after incubation at 30°C for two days (for wild-type selection)
583 or four days (for pph22Δ and dual-resistant fusion products). Fusion frequency was calculated
584 as the number of CFUs on YPD+NAT+NEO divided by the total number of colonies on
585 YPD+NAT and YPD+NEO, and expressed as a percentage relative to the wild-type control.
586 Each assay was performed in triplicate.
587
588 **Flow cytometry**
589 For ploidy determination of *Cryptococcus* samples, fluorescence activated cell sorting
590 (FACS) was performed according to a previously published protocol, with slight modifications
591 [62]. Wild-type and mutant strains were grown on YPD plate medium at 30ºC overnight,
592 harvested, and washed with PBS. The cells were then fixed in 70% ethanol for 16 hours at 4ºC.
593 Fixed cells were pelleted and washed with 1 mL NS buffer (10 mM Tris-HCl, 0.25 M sucrose, 1
594 mM EDTA, 1 mM $MgCl_2$, 0.1 mM $ZnCl_2$, 0.4 mM phenylmethylsulfonyl fluoride, and 7 mM β-
595 mercaptoethanol). After centrifugation, the cells were treated with RNase (0.5 mg/mL) and
596 stained with propidium iodide (10 μg/mL) in a 200 μL suspension of NS buffer for 2 hours in the
597 dark. Then, 50 μL of the stained cells were diluted into 200 μL of 50 mM Tris-HCl, pH=8.0, and
598 submitted to the Duke Cancer Institute Flow Cytometry Shared Resource for analysis.
599 Fluorescence was measured using a BD FACSCanto flow cytometer and analyzed with BD
600 FACSDiva software. Approximately 15,000 to 20,000 events were analyzed for each sample.
601
602 **Whole-genome sequencing and SNP analysis**
603 Genomic DNA for whole-genome sequencing was extracted from saturated 4 mL YPD
604 cultures with the MasterPure Yeast DNA Purification Kit. The precipitated DNA was dissolved in
605 35 μL of 1x TE buffer (100 mM Tris-HCl, 10 mM EDTA, pH=8.0), and the concentration was
606 estimated using Qubit. Illumina sequencing was performed at the Duke Sequencing and
607 Genomic Technologies core facility (https://genome.duke.edu) with Novaseq X Plus, providing

250 bp paired-end reads. The Illumina sequences were trimmed using trim-galore (v 0.6.7) and mapped to the H99α genome assembly (RefSeq: GCF_000149245.1) using Geneious software. The resulting BAM files were converted to TDF format, and read coverage was visualized in IGV to verify uniform read coverage across the genome**.** For SNP calling, the Illumina sequences were mapped to the H99α genome assembly using the Geneious default mapper with five iterations. Variant calling was performed with BAM mapped read files, with parameters set to a 0.9 variant frequency and a minimum of 100x coverage per variant. For the KN99**a**/KN99α diploid strain (CnLC6683), variant calling was performed with a 0.45 frequency and 100x coverage per variant. Illumina sequences from H99α and KN99**a**/KN99α served as controls for SNP calling analysis. Variants were exported from Geneious as VCF files and imported into IGV for visualization.

Quantification and statistical analysis

All statistical analyses and data visualizations were performed with GraphPad Prism v10 software. Details regarding replication, quantification, and statistical tests used for each experiment are provided in the methods and corresponding figure legends.

References

1. Goudreault M, D'Ambrosio LM, Kean MJ, Mullin MJ, Larsen BG, Sanchez A, et al. A PP2A phosphatase high density interaction network identifies a novel striatin-interacting phosphatase and kinase complex linked to the cerebral cavernous malformation 3 (CCM3) protein. Mol Cell Proteomics. 2009;8(1):157-71. Epub 2008/09/11. doi: 10.1074/mcp.M800266-MCP200. PubMed PMID: 18782753; PubMed Central PMCID: 2621004.
2. Neisch AL, Neufeld TP, Hays TS. A STRIPAK complex mediates axonal transport of autophagosomes and dense core vesicles through PP2A regulation. J Cell Biol. 2017;216(2):441-61. Epub 2017/01/20. doi: 10.1083/jcb.201606082. PubMed PMID: 28100687; PubMed Central PMCID: PMC5294782.
3. Li D, Musante V, Zhou W, Picciotto MR, Nairn AC. Striatin-1 is a B subunit of protein phosphatase PP2A that regulates dendritic arborization and spine development in striatal neurons. J Biol Chem. 2018;293(28):11179-94. Epub 2018/05/29. doi: 10.1074/jbc.RA117.001519. PubMed PMID: 29802198; PubMed Central PMCID: PMC6052221.
4. Gordon J, Hwang J, Carrier KJ, Jones CA, Kern QL, Moreno CS, et al. Protein phosphatase 2a (PP2A) binds within the oligomerization domain of striatin and regulates the phosphorylation and activation of the mammalian Ste20-Like kinase Mst3. BMC Biochemistry. 2011;12:54. doi: 10.1186/1471-2091-12-54. PubMed PMID: 21985334; PubMed Central PMCID: 3217859.
5. Janssens V, Goris J. Protein phosphatase 2A: a highly regulated family of serine/threonine phosphatases implicated in cell growth and signalling. Biochem J. 2001;353(Pt 3):417-39. doi: 10.1042/0264-6021:3530417. PubMed PMID: 11171037; PubMed Central PMCID: PMC1221586.
6. Cho US, Xu W. Crystal structure of a protein phosphatase 2A heterotrimeric holoenzyme. Nature. 2007;445(7123):53-7. Epub 20061101. doi: 10.1038/nature05351. PubMed PMID: 17086192.
7. Sandal P, Jong CJ, Merrill RA, Song J, Strack S. Protein phosphatase 2A - structure, function and role in neurodevelopmental disorders. J Cell Sci. 2021;134(13). Epub 20210706. doi: 10.1242/jcs.248187. PubMed PMID: 34228795; PubMed Central PMCID: PMC8277144.
8. Sents W, Ivanova E, Lambrecht C, Haesen D, Janssens V. The biogenesis of active protein phosphatase 2A holoenzymes: a tightly regulated process creating phosphatase specificity. FEBS J. 2013;280(2):644-61. Epub 20120425. doi: 10.1111/j.1742-4658.2012.08579.x. PubMed PMID: 22443683.
9. Ribeiro PS, Josue F, Wepf A, Wehr MC, Rinner O, Kelly G, et al. Combined functional genomic and proteomic approaches identify a PP2A complex as a negative regulator of Hippo signaling. Mol Cell. 2010;39(4):521-34. Epub 2010/08/28. doi: 10.1016/j.molcel.2010.08.002. PubMed PMID: 20797625.
10. Kuck U, Radchenko D, Teichert I. STRIPAK, a highly conserved signaling complex, controls multiple eukaryotic cellular and developmental processes and is linked with human diseases. Biol Chem. 2019. Epub 2019/05/03. doi: 10.1515/hsz-2019-0173. PubMed PMID: 31042639.
11. Kuck U, Poggeler S. STRIPAK, a fundamental signaling hub of eukaryotic development. Microbiol Mol Biol Rev. 2024;88(4):e0020523. Epub 20241111. doi: 10.1128/mmbr.00205-23. PubMed PMID: 39526753; PubMed Central PMCID: PMC11653735.
12. Jeong BC, Bae SJ, Ni L, Zhang X, Bai XC, Luo X. Cryo-EM structure of the Hippo signaling integrator human STRIPAK. Nature Structural & Molecular Biology.

674 2021;28(3):290-9. Epub 2021/02/27. doi: 10.1038/s41594-021-00564-y. PubMed PMID:
675 33633399; PubMed Central PMCID: PMC8315899.
676 13. Shi Z, Jiao S, Zhou Z. STRIPAK complexes in cell signaling and cancer. Oncogene.
677 2016;35(35):4549-57. Epub 2016/02/16. doi: 10.1038/onc.2016.9. PubMed PMID:
678 26876214.
679 14. Bernhards Y, Poggeler S. The phocein homologue SmMOB3 is essential for vegetative
680 cell fusion and sexual development in the filamentous ascomycete *Sordaria macrospora*.
681 Curr Genet. 2011;57(2):133-49. Epub 20110113. doi: 10.1007/s00294-010-0333-z.
682 PubMed PMID: 21229248; PubMed Central PMCID: PMC3059760.
683 15. Bloemendal S, Bernhards Y, Bartho K, Dettmann A, Voigt O, Teichert I, et al. A
684 homologue of the human STRIPAK complex controls sexual development in fungi. Mol
685 Microbiol. 2012;84(2):310-23. doi: 10.1111/j.1365-2958.2012.08024.x. PubMed PMID:
686 22375702.
687 16. Kuck U, Stein V. STRIPAK, a Key Regulator of Fungal Development, Operates as a
688 Multifunctional Signaling Hub. J Fungi. 2021;7(6):443. Epub 2021/07/03. doi:
689 10.3390/jof7060443. PubMed PMID: 34206073; PubMed Central PMCID: PMC8226480.
690 17. Chen A, Liu N, Xu C, Wu S, Liu C, Qi H, et al. The STRIPAK complex orchestrates cell
691 wall integrity signalling to govern the fungal development and virulence of *Fusarium*
692 *graminearum*. Mol Plant Pathol. 2023;24(9):1139-53. Epub 20230606. doi:
693 10.1111/mpp.13359. PubMed PMID: 37278525; PubMed Central PMCID:
694 PMC10423325.
695 18. Pracheil T, Thornton J, Liu Z. TORC2 signaling is antagonized by protein phosphatase
696 2A and the Far complex in *Saccharomyces cerevisiae*. Genetics. 2012;190(4):1325-39.
697 doi: 10.1534/genetics.111.138305. PubMed PMID: 22298706; PubMed Central PMCID:
698 3316646.
699 19. Pracheil T, Liu Z. Tiered assembly of the yeast Far3-7-8-9-10-11 complex at the
700 endoplasmic reticulum. J Biol Chem. 2013;288(23):16986-97. doi:
701 10.1074/jbc.M113.451674. PubMed PMID: 23625923; PubMed Central PMCID:
702 3675630.
703 20. Frost A, Elgort MG, Brandman O, Ives C, Collins SR, Miller-Vedam L, et al. Functional
704 repurposing revealed by comparing *S. pombe* and *S. cerevisiae* genetic interactions.
705 Cell. 2012;149(6):1339-52. doi: 10.1016/j.cell.2012.04.028. PubMed PMID: 22682253.
706 21. Poggeler S, Kuck U. A WD40 repeat protein regulates fungal cell differentiation and can
707 be replaced functionally by the mammalian homologue striatin. Eukaryot Cell.
708 2004;3(1):232-40. doi: 10.1128/EC.3.1.232-240.2004. PubMed PMID: 14871953;
709 PubMed Central PMCID: PMC329509.
710 22. Dettmann A, Heilig Y, Ludwig S, Schmitt K, Illgen J, Fleissner A, et al. HAM-2 and HAM-3
711 are central for the assembly of the *Neurospora* STRIPAK complex at the nuclear
712 envelope and regulate nuclear accumulation of the MAP kinase MAK-1 in a MAK-2-
713 dependent manner. Mol Microbiol. 2013;90(4):796-812. Epub 2013/09/14. doi:
714 10.1111/mmi.12399. PubMed PMID: 24028079.
715 23. Wang CL, Shim WB, Shaw BD. *Aspergillus nidulans* striatin (StrA) mediates sexual
716 development and localizes to the endoplasmic reticulum. Fungal Genet Biol.
717 2010;47(10):789-99. Epub 20100626. doi: 10.1016/j.fgb.2010.06.007. PubMed PMID:
718 20601045.
719 24. Elramli N, Karahoda B, Sarikaya-Bayram O, Frawley D, Ulas M, Oakley CE, et al.
720 Assembly of a heptameric STRIPAK complex is required for coordination of light-
721 dependent multicellular fungal development with secondary metabolism in *Aspergillus*
722 *nidulans*. PLoS Genet. 2019;15(3):e1008053. Epub 2019/03/19. doi:
723 10.1371/journal.pgen.1008053. PubMed PMID: 30883543; PubMed Central PMCID:
724 PMC6438568.

25. Islam KT, Bond JP, Fakhoury AM. FvSTR1, a striatin orthologue in *Fusarium virguliforme*, is required for asexual development and virulence. Appl Microbiol Biotechnol. 2017;101(16):6431-45. Epub 2017/06/24. doi: 10.1007/s00253-017-8387-1. PubMed PMID: 28643182.
26. Yamamura Y, Shim WB. The coiled-coil protein-binding motif in *Fusarium verticillioides* Fsr1 is essential for maize stalk rot virulence. Microbiology. 2008;154(Pt 6):1637-45. doi: 10.1099/mic.0.2008/016782-0. PubMed PMID: 18524918.
27. Wang CL, Shim WB, Shaw BD. The *Colletotrichum graminicola* striatin orthologue Str1 is necessary for anastomosis and is a virulence factor. Mol Plant Pathol. 2016;17(6):931-42. Epub 20160218. doi: 10.1111/mpp.12339. PubMed PMID: 26576029; PubMed Central PMCID: PMC6638439.
28. Schmidpeter J, Dahl M, Hofmann J, Koch C. ChMob2 binds to ChCbk1 and promotes virulence and conidiation of the fungal pathogen *Colletotrichum higginsianum*. BMC Microbiol. 2017;17(1):22. Epub 20170119. doi: 10.1186/s12866-017-0932-7. PubMed PMID: 28103800; PubMed Central PMCID: PMC5248491.
29. Kim MS, Zhang H, Yan H, Yoon BJ, Shim WB. Characterizing co-expression networks underpinning maize stalk rot virulence in *Fusarium verticillioides* through computational subnetwork module analyses. Sci Rep. 2018;8(1):8310. Epub 20180529. doi: 10.1038/s41598-018-26505-2. PubMed PMID: 29844502; PubMed Central PMCID: PMC5974142.
30. Peterson PP, Choi JT, Fu C, Cowen LE, Sun S, Bahn YS, et al. The *Cryptococcus neoformans* STRIPAK complex controls genome stability, sexual development, and virulence. PLoS Pathog. 2024;20(11):e1012735. Epub 20241119. doi: 10.1371/journal.ppat.1012735. PubMed PMID: 39561188; PubMed Central PMCID: PMC11614259.
31. Giles SS, Dagenais TR, Botts MR, Keller NP, Hull CM. Elucidating the pathogenesis of spores from the human fungal pathogen *Cryptococcus neoformans*. Infect Immun. 2009;77(8):3491-500. Epub 20090518. doi: 10.1128/IAI.00334-09. PubMed PMID: 19451235; PubMed Central PMCID: PMC2715683.
32. Velagapudi R, Hsueh YP, Geunes-Boyer S, Wright JR, Heitman J. Spores as infectious propagules of *Cryptococcus neoformans*. Infect Immun. 2009;77(10):4345-55. Epub 2009/07/22. doi: 10.1128/IAI.00542-09. PubMed PMID: 19620339; PubMed Central PMCID: PMC2747963.
33. Kwon-Chung KJ, Edman JC, Wickes BL. Genetic association of mating types and virulence in *Cryptococcus neoformans*. Infect Immun. 1992;60(2):602-5. doi: 10.1128/iai.60.2.602-605.1992. PubMed PMID: 1730495; PubMed Central PMCID: PMC257671.
34. Zhao Y, Lin J, Fan Y, Lin X. Life Cycle of *Cryptococcus neoformans*. Annu Rev Microbiol. 2019;73:17-42. Epub 20190513. doi: 10.1146/annurev-micro-020518-120210. PubMed PMID: 31082304.
35. Sun S, Coelho MA, David-Palma M, Priest SJ, Heitman J. The evolution of sexual reproduction and the mating-type locus: links to pathogenesis of *Cryptococcus* human pathogenic fungi. Annu Rev Genet. 2019;53:417-44. Epub 2019/09/21. doi: 10.1146/annurev-genet-120116-024755. PubMed PMID: 31537103; PubMed Central PMCID: PMC7025156.
36. Hull CM, Heitman J. Genetics of *Cryptococcus neoformans*. Annu Rev Genet. 2002;36:557-615. Epub 2002/11/14. doi: 10.1146/annurev.genet.36.052402.152652. PubMed PMID: 12429703.
37. Idnurm A. A tetrad analysis of the basidiomycete fungus *Cryptococcus neoformans*. Genetics. 2010;185(1):153-63. Epub 20100215. doi: 10.1534/genetics.109.113027. PubMed PMID: 20157004; PubMed Central PMCID: PMC2870951.

38. Yadav V, Sun S, Heitman J. Uniparental nuclear inheritance following bisexual mating in fungi. eLife. 2021;10. Epub 2021/08/03. doi: 10.7554/eLife.66234. PubMed PMID: 34338631; PubMed Central PMCID: PMC8412948.
39. Yan Z, Xu J. Mitochondria are inherited from the *MAT*a parent in crosses of the basidiomycete fungus *Cryptococcus neoformans*. Genetics. 2003;163(4):1315-25. doi: 10.1093/genetics/163.4.1315. PubMed PMID: 12702677; PubMed Central PMCID: PMC1462512.
40. Lavanchy G, Schwander T. Hybridogenesis. Curr Biol. 2019;29(3):539. doi: 10.1016/j.cub.2019.01.020. PubMed PMID: 30721675.
41. Casselton LA, Olesnicky NS. Molecular genetics of mating recognition in basidiomycete fungi. Microbiol Mol Biol Rev. 1998;62(1):55-70. doi: 10.1128/MMBR.62.1.55-70.1998. PubMed PMID: 9529887; PubMed Central PMCID: PMC98906.
42. Kozubowski L, Heitman J. Septins enforce morphogenetic events during sexual reproduction and contribute to virulence of *Cryptococcus neoformans*. Mol Microbiol. 2010;75(3):658-75. Epub 2009/12/01. doi: 10.1111/j.1365-2958.2009.06983.x. PubMed PMID: 19943902; PubMed Central PMCID: PMC3699866.
43. Lin X, Hull CM, Heitman J. Sexual reproduction between partners of the same mating type in *Cryptococcus neoformans*. Nature. 2005;434(7036):1017-21. Epub 2005/04/23. doi: 10.1038/nature03448. PubMed PMID: 15846346.
44. Xu J, Ali RY, Gregory DA, Amick D, Lambert SE, Yoell HJ, et al. Uniparental mitochondrial transmission in sexual crosses in *Cryptococcus neoformans*. Curr Microbiol. 2000;40(4):269-73. doi: 10.1007/s002849910053. PubMed PMID: 10688697.
45. Matha AR, Lin X. Current perspectives on uniparental mitochondrial inheritance in *Cryptococcus neoformans*. Pathogens. 2020;9(9). Epub 20200910. doi: 10.3390/pathogens9090743. PubMed PMID: 32927641; PubMed Central PMCID: PMC7559238.
46. Nielsen K, Cox GM, Wang P, Toffaletti DL, Perfect JR, Heitman J. Sexual cycle of *Cryptococcus neoformans* var. *grubii* and virulence of congenic a and alpha isolates. Infect Immun. 2003;71(9):4831-41. Epub 2003/08/23. doi: 10.1128/IAI.71.9.4831-4841.2003. PubMed PMID: 12933823; PubMed Central PMCID: PMC187335.
47. Janbon G, Ormerod KL, Paulet D, Byrnes EJ, 3rd, Yadav V, Chatterjee G, et al. Analysis of the genome and transcriptome of *Cryptococcus neoformans* var. *grubii* reveals complex RNA expression and microevolution leading to virulence attenuation. PLoS Genet. 2014;10(4):e1004261. Epub 2014/04/20. doi: 10.1371/journal.pgen.1004261. PubMed PMID: 24743168; PubMed Central PMCID: PMC3990503.
48. Arras SDM, Ormerod KL, Erpf PE, Espinosa MI, Carpenter AC, Blundell RD, et al. Convergent microevolution of *Cryptococcus neoformans* hypervirulence in the laboratory and the clinic. Sci Rep. 2017;7(1):17918. Epub 20171220. doi: 10.1038/s41598-017-18106-2. PubMed PMID: 29263343; PubMed Central PMCID: PMC5738413.
49. Arras SD, Chitty JL, Blake KL, Schulz BL, Fraser JA. A genomic safe haven for mutant complementation in *Cryptococcus neoformans*. PLoS One. 2015;10(4):e0122916. Epub 20150409. doi: 10.1371/journal.pone.0122916. PubMed PMID: 25856300; PubMed Central PMCID: PMC4391909.
50. Abramson J, Adler J, Dunger J, Evans R, Green T, Pritzel A, et al. Accurate structure prediction of biomolecular interactions with AlphaFold 3. Nature. 2024;630(8016):493-500. Epub 20240508. doi: 10.1038/s41586-024-07487-w. PubMed PMID: 38718835; PubMed Central PMCID: PMC11168924.
51. Mirdita M, Schütze K, Moriwaki Y, Heo L, Ovchinnikov S, Steinegger M. ColabFold: Making Protein folding accessible to all. Nature Methods. 2022. doi: 10.1038/s41592-022-01488-1.

52. Yadav V, Sun S, Heitman J. On the evolution of variation in sexual reproduction through the prism of eukaryotic microbes. Proc Natl Acad Sci U S A. 2023;120(10):e2219120120. Epub 20230303. doi: 10.1073/pnas.2219120120. PubMed PMID: 36867686; PubMed Central PMCID: PMC10013875.
53. Fu C, Sun S, Billmyre RB, Roach KC, Heitman J. Unisexual versus bisexual mating in *Cryptococcus neoformans*: Consequences and biological impacts. Fungal Genet Biol. 2015;78:65-75. Epub 2014/09/01. doi: 10.1016/j.fgb.2014.08.008. PubMed PMID: 25173822; PubMed Central PMCID: PMC4344436.
54. Sakuma C, Saito Y, Umehara T, Kamimura K, Maeda N, Mosca TJ, et al. The Strip-Hippo pathway regulates synaptic terminal formation by modulating actin organization at the *Drosophila* neuromuscular synapses. Cell Reports. 2016;16(9):2289-97. Epub 2016/08/23. doi: 10.1016/j.celrep.2016.07.066. PubMed PMID: 27545887; PubMed Central PMCID: PMC5023852.
55. Gupta R, Kumar G, Jain BP, Chandra S, Goswami SK. Ectopic expression of 35 kDa and knocking down of 78 kDa SG2NAs induce cytoskeletal reorganization, alter membrane sialylation, and modulate the markers of EMT. Mol Cell Biochem. 2021;476(2):633-48. Epub 2020/10/22. doi: 10.1007/s11010-020-03932-2. PubMed PMID: 33083950.
56. Wernet V, Wackerle J, Fischer R. The STRIPAK component SipC is involved in morphology and cell-fate determination in the nematode-trapping fungus *Duddingtonia flagrans*. Genetics. 2022;220(1). Epub 2021/12/02. doi: 10.1093/genetics/iyab153. PubMed PMID: 34849851; PubMed Central PMCID: PMC8733638.
57. Jacinto E, Loewith R, Schmidt A, Lin S, Ruegg MA, Hall A, et al. Mammalian TOR complex 2 controls the actin cytoskeleton and is rapamycin insensitive. Nat Cell Biol. 2004;6(11):1122-8. PubMed PMID: 15467718.
58. Fan Y, Lin X. Multiple applications of a transient CRISPR-Cas9 coupled with electroporation (TRACE) system in the *Cryptococcus neoformans* species complex. Genetics. 2018;208(4):1357-72. Epub 20180214. doi: 10.1534/genetics.117.300656. PubMed PMID: 29444806; PubMed Central PMCID: PMC5887135.
59. Huang MY, Joshi MB, Boucher MJ, Lee S, Loza LC, Gaylord EA, et al. Short homology-directed repair using optimized Cas9 in the pathogen *Cryptococcus neoformans* enables rapid gene deletion and tagging. Genetics. 2022;220(1). doi: 10.1093/genetics/iyab180. PubMed PMID: 34791226; PubMed Central PMCID: PMC8733451.
60. Lin X, Chacko N, Wang L, Pavuluri Y. Generation of stable mutants and targeted gene deletion strains in *Cryptococcus neoformans* through electroporation. Med Mycol. 2015;53(3):225-34. Epub 20141224. doi: 10.1093/mmy/myu083. PubMed PMID: 25541555; PubMed Central PMCID: PMC4574871.
61. Davidson RC, Cruz MC, Sia RA, Allen B, Alspaugh JA, Heitman J. Gene disruption by biolistic transformation in serotype D strains of *Cryptococcus neoformans*. Fungal Genet Biol. 2000;29(1):38-48. Epub 2000/04/26. doi: 10.1006/fgbi.1999.1180. PubMed PMID: 10779398.
62. Tanaka R, Taguchi H, Takeo K, Miyaji M, Nishimura K. Determination of ploidy in *Cryptococcus neoformans* by flow cytometry. J Med Vet Mycol. 1996;34(5):299-301. PubMed PMID: 8912162.

871 **Figure legends**

872 **Figure 1.** *pph22*Δ x wild type crosses exhibit unusual sexual development. A) Mating efficiency
873 of *pph22*Δ strains crossed with wild-type of the opposite mating type (H99α or KN99**a**). Images
874 were taken between 4 to 6 weeks of incubation on MS plates. Scale bars in the middle and
875 bottom panels are 200 μm and 20 μm, respectively. B) Scanning electron microscopy (SEM) of
876 sexual structures in WT x WT and *pph22*Δ x WT crosses showing examples of a hyphal filament
877 terminating in a basidial head and basidiospores emerging from a basidium. The clamp cells
878 (white arrowheads) in the wild-type cross are fused to the subapical cell in the elongating hypha.
879 In *pph22*Δ x WT crosses, both fused and unfused clamp cells were often observed along the
880 same hypha. Scale bars in each panel represent 5 μm.

881

882 **Figure 2.** Progeny from *pph22*Δ x wild type exhibit uniparental nuclear inheritance from H99α
883 and lack evidence of meiotic recombination. Whole-genome sequencing followed by SNP
884 analysis revealed no contribution of the KN99**a** *pph22*Δ parental genome, as evidenced by the
885 absence of SNPs compared to the H99α reference genome. The three known polymorphic
886 regions distinguishing H99 and KN99 background strains are located on chromosomes 5 (the
887 mating-type locus), 11, and 14. These regions are highlighted in the lower panels, with the
888 chromosomal coordinates labeled accordingly. The KN99**a**/KN99α diploid strain (CnLC6683),
889 from which KN99**a** *pph22*Δ was obtained, was used as a control for variant calling. The few
890 SNPs identified in the progeny were restricted to nucleotide repeat regions. Mitochondrial
891 haplotypes were determined based on the presence or absence of an intron in the *COX1* gene
892 from whole-genome sequencing reads. “Germ.” stands for the germination frequency of the
893 indicated basidium and “P” stands for progeny.

894

895 **Figure 3.** Fluorescence microscopy depicts loss of one parental nucleus following hyphal
896 branching during pseudosexual reproduction. A) Loss of the wild-type nucleus at a hyphal
897 branch point in *pph22*Δ Nop1-GFP x WT Nop1-RFP. B) and C) Inheritance of only the *pph22*Δ
898 nucleus in basidiospores, which appear collapsed on the basidial head and have an irregular
899 morphology, is observed after loss of the WT nucleus in a hyphal compartment (B) and following
900 branching (C). D) Loss of the wild-type nucleus and retention of the *pph22*Δ nucleus results in
901 severely abnormal hyphal development (white arrowhead). In another hyphal branch, both
902 nuclei have undergone division in the dikaryon without segregating into separate hyphal cells
903 (grey arrowheads). The white arrowheads indicate the point in the hypha where one parental
904 nucleus is lost. The scale bar in each panel represents 5 µm.

905

906 **Figure 4.** The *pph22*Δ *suppressor* strains are restored for α-**a** sexual mating in crosses with wild
907 type. A) Mating efficiencies in wild-type and *pph22*Δ *sup* crosses. Hyphal production and
908 elongation, and sporulation were observed to similar extents. B) Germination of spores
909 dissected from *pph22*Δ *sup* x WT after two days of incubation on YPD. Each row depicts spores
910 from separate basidia. Colonies that grew on YPD+NAT (containing the *pph22*Δ*::NAT* mutant
911 allele) are indicated by the white boxes. C) Genotyping analysis of progeny dissected from
912 *pph22*Δ *sup* strains crossed with the KN99**a** strain bearing recombinant mitochondria (SSH118).
913 Each spot is from a separate mating patch and is considered an independent experiment.

914

915 **Figure 5.** Overexpression of *PPG1* suppresses the *pph22*Δ mutation. A) Germination of spores
916 dissected from a *PPH22/pph22*Δ heterozygous mutant diploid strain expressing *TEF1-PPG1*
917 (*PPG1-OE)* on YPD. The genotypes of the colonies indicated were determined from growth on
918 YPD+NAT (*pph22*Δ::*NAT* allele) and YPD+NAT+NEO (*pph22*Δ*::NAT* and P_{TEF1}*-PPG1-NEO*

919 alleles). B) The indicated strains were serially diluted and grown on YPD solid media at 25ºC,
920 30ºC, and 37ºC; or YPD supplemented with 1 M sorbitol, 100 ng/mL rapamycin, 1 µg/mL FK506,
921 or 100 µg/mL cyclosporine A, each at 30ºC. Images were taken after three days incubation. C)
922 Strains were grown in liquid culture overnight in YPD at 30ºC and plated onto Niger seed agar.
923 Images were captured after four days. D) Analysis of capsule formation by India ink staining.
924 The indicated strains were grown for 3 days in RPMI media at 30ºC. Images are representative
925 of two biological replicates. Scale bar is 5 µm. E) Mating of *ppg1*Δ and *pph22*Δ *PPG1-OE*
926 strains crossed to wild type on MS media. Images were taken after six weeks. White
927 arrowheads indicate bald basidia heads that did not produce spores. The scale bars in the
928 middle and bottom panels are 200 µm and 50 µm.

929

930 **Figure 6.** *far8*Δ mutants also display a high rate of pseudosexual reproduction. A) SEM of
931 mated wild-type and *far8*Δ shows two basidia heads producing spores with abnormal
932 morphology. In the basidium on the right, spores are seen budding from seven independent
933 spots on the basidial head. The scale bar represents 5 µm. B) Dissection of spores from *far8*Δ x
934 WT yields colonies mostly homogenous in size on YPD. *far8*Δ mutants were identified based on
935 growth on YPD+NEO and form smaller, slow-growing colonies compared to wild type. Each row
936 of spores is from an independent basidium. C) Genotyping analysis of progeny from individual
937 basidia in *far8*Δ x WT crosses. Each spot analyzed is from an independent mating experiment.

938

Figure 1

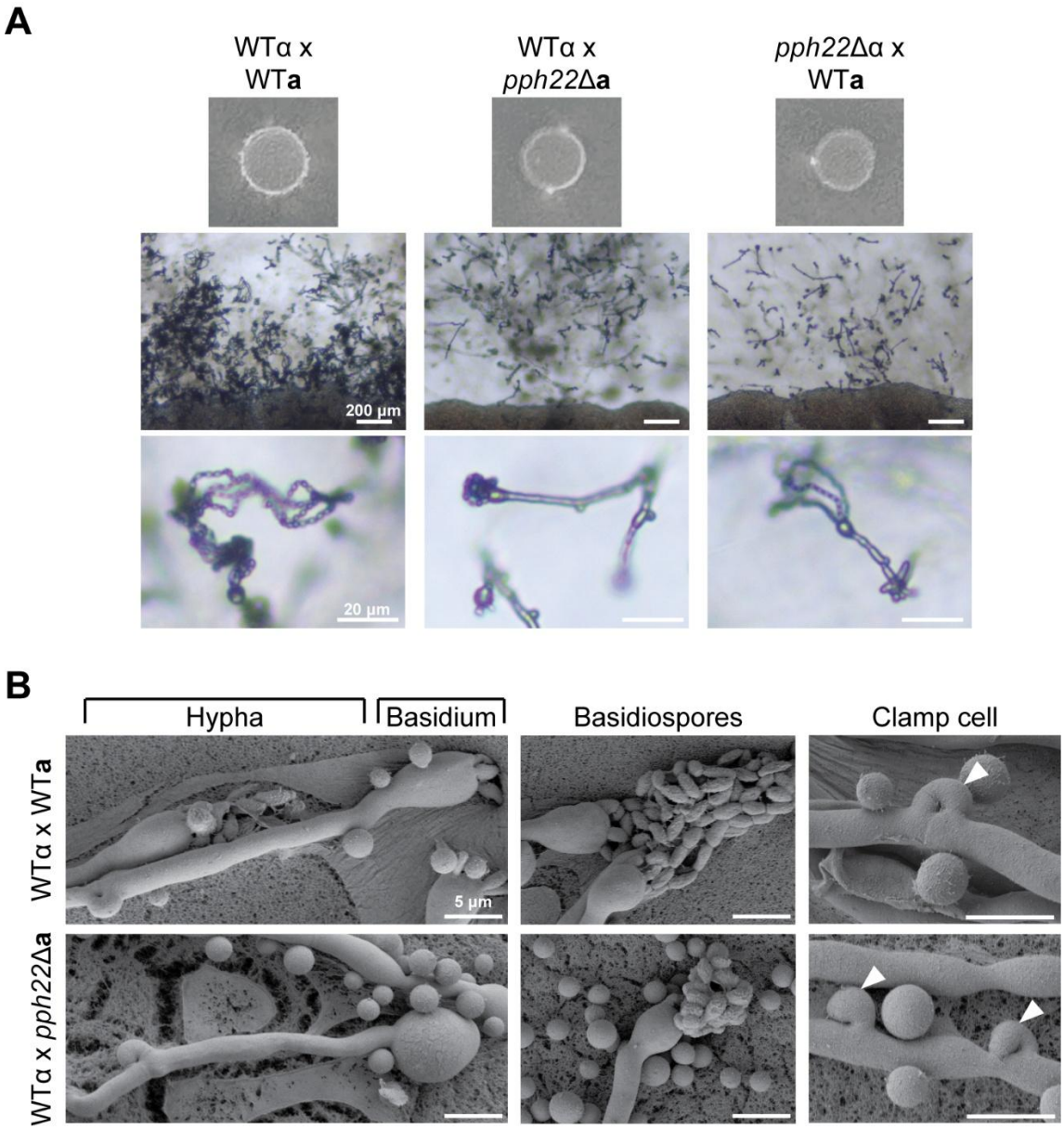
A
WTα x
WTa
WTα x
pph22Δa
pph22Δα x
WTa
200 µm
20 µm
B
Hypha
Basidium
Basidiospores
Clamp cell
WTα x WTa
WTα x pph22Δa
5 µm

Table 1. Genotyping analysis of spores from individual basidia and from random spore dissection in *pph22*Δ x wild type crosses. Spot refers to the individual mating spot from which those basidia were dissected in the indicated crosses, with each spot being an independent experiment. Mito. refers to mitochondria.

Spot	Basidia #	Spores germinated/dissected	% Germination	NAT^R	*MAT*	Mito.
pph22Δ::NAT **a** (PP56) x H99α						
A	1	13/14	93	0	All α	**a**
	2	1/14	7	0	All α	**a**
	3	13/14	93	0	All α	**a**
	4	3/9	33	0	All α	**a**
	5	14/14	100	0	All α	**a**
B	6	14/28	50	0	All α	α
	7	26/28	93	0	All α	α
	8	10/16	63	0	All α	α
	9	16/23	70	0	All α	α
	10	27/27	100	0	All α	α
	11	13/14	93	0	All α	α
C	12	11/14	79	0	All α	**a**
	13	13/14	93	0	All α	**a**
	14	14/14	100	0	All α	**a**
pph22Δ::NAT **a** (PP58) x H99α						
D	1	12/14	86	0	All α	**a**
	2	14/14	100	0	All α	α
	3	14/14	100	0	All α	**a**
	4	13/14	93	0	All α	**a**
	5	11/14	79	0	All α	**a**
E	6	13/14	93	0	All α	**a**
	7	14/14	100	0	All α	**a**
	8	3/9	33	0	All α	**a**
pph22Δ::NAT α (PP53) x KN99**a**						
F	1	26/28	93	0	All a	**a**
	2	8/18	44	0	All **a**	**a**
	3	18/28	64	0	All **a**	**a**
	4	16/17	94	0	All **a**	**a**
	5	18/22	82	0	All **a**	**a**
	6	26/50	52	0	All **a**	**a**

Random spore dissection

Spot	Spore #	NAT^R	*MAT*	Mito.
pph22Δ::NAT **a** (PP58) x H99α				
G	1-50	0	All α	**a**
H	51-65	0	All α	α

Figure 2

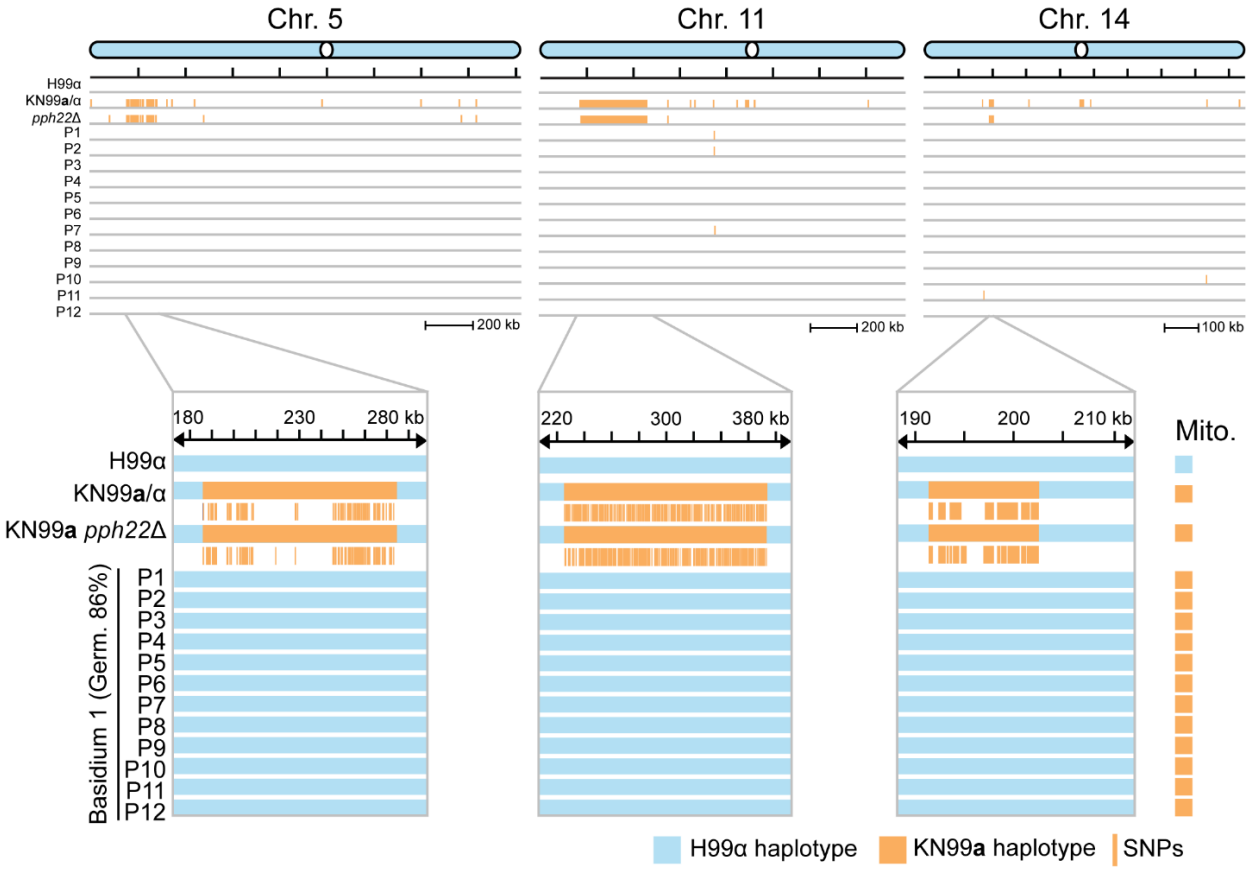
Chr. 5
Chr. 11
Chr. 14
H99α
KN99a/α
pph22Δ
P1
P2
P3
P4
P5
P6
P7
P8
P9
P10
P11
P12
200 kb
200 kb
100 kb
180
230
280 kb
220
300
380 kb
190
200
210 kb
Mito.
H99α
KN99a/α
KN99a pph22Δ
Basidium 1 (Germ. 86%)
H99α haplotype
KN99a haplotype
SNPs

Figure 3

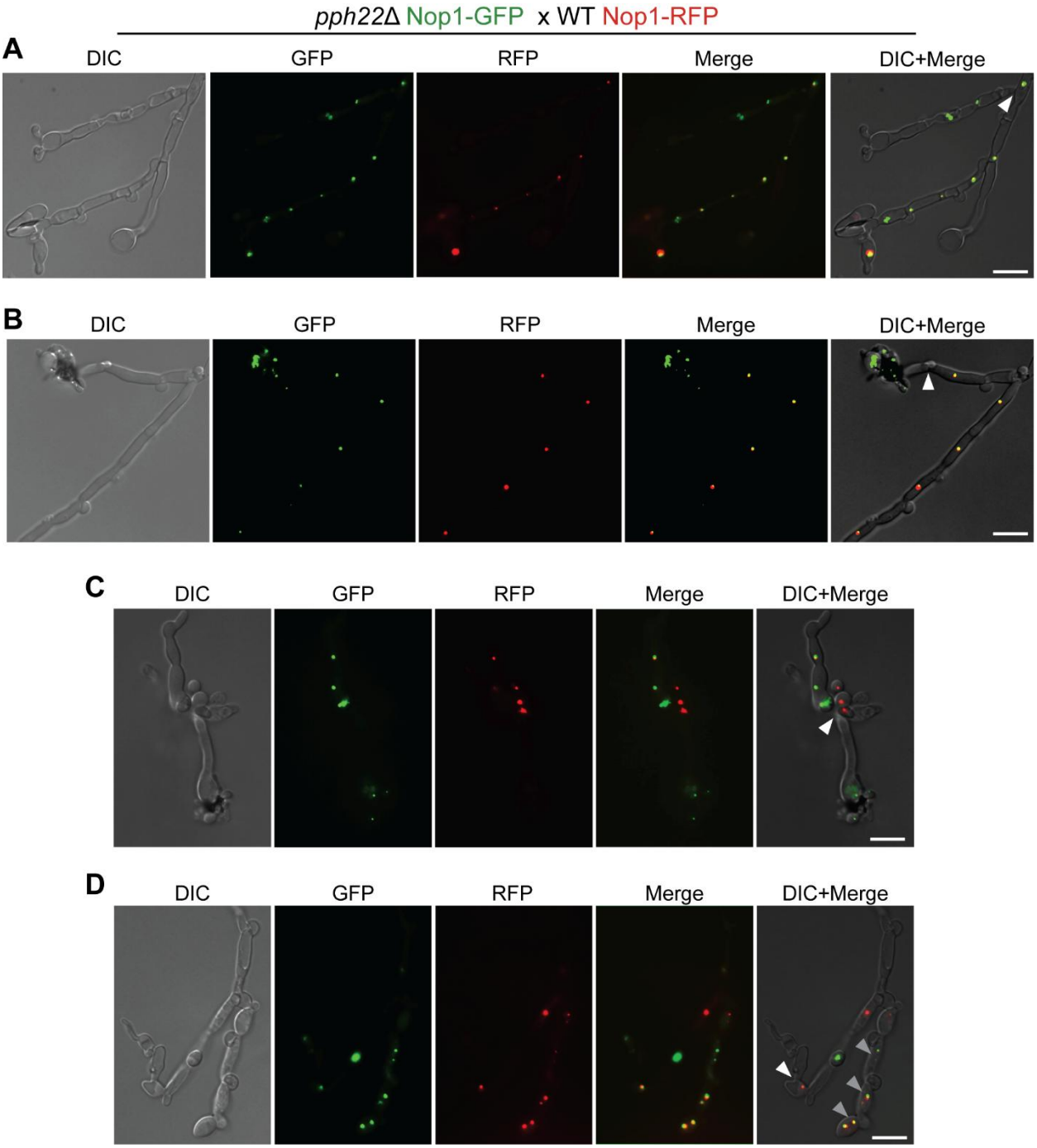
*pph22*Δ Nop1-GFP x WT Nop1-RFP
A
DIC
GFP
RFP
Merge
DIC+Merge
B
DIC
GFP
RFP
Merge
DIC+Merge
C
DIC
GFP
RFP
Merge
DIC+Merge
D
DIC
GFP
RFP
Merge
DIC+Merge

Figure 4

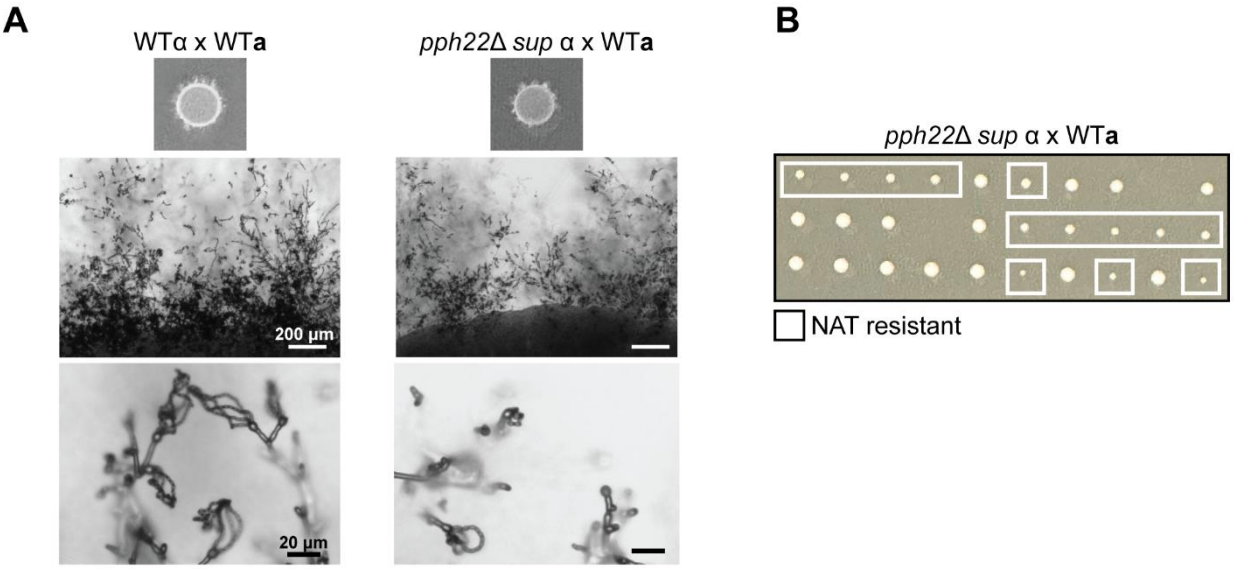

C

Spot	Basidia #	Spores germinated/dissected	% Germination	NAT^R	*MAT*	Mito.
pph22Δ::NAT sup α (PP80) x KN99**a** (SSH118)						
A	1	8/9	89	0	1 α, 7 α/**a**	**a**
B	2	10/14	71	0	3 α, 7 α/**a**	**a**
C	3	10/14	71	0	1 α, 9 α/**a**	**a**
D	4	13/14	93	0	1 **a**, 2 α, 10 α/**a**	**a**
E	5	10/10	100	0	10 **a**	**a**
F	6	12/12	100	0	12 **a**	**a**
G	7	13/14	93	0	5 **a**, 8 α/**a**	**a**
H	8	13/14	93	0	4 **a**, 9 α/**a**	**a**
I	9	10/10	100	0	10 **a**	**a**
J	10	14/14	100	0	6 **a**, 8 α/**a**	**a**
K	11	14/14	100	0	4 **a**, 10 α/**a**	**a**
L	12	7/7	100	0	2 **a**, 5 α/**a**	**a**
pph22Δ::NAT sup α (PP84) x KN99**a** (SSH118)						
A	1	12/12	100	7	3 **a**, 4 α, 5 α/**a**	**a**
B	2	8/14	57	6	2 **a**, 6 α/**a**	**a**
C	3	11/14	79	7	5 **a**, 6 α/**a**	**a**
D	4	13/14	93	6	5 **a**, 2 α, 6 α/**a**	**a**
E	5	14/14	100	3	2 **a**, 2 α, 10 α/**a**	**a**
F	6	9/14	64	3	2 **a**, 7 α/**a**	**a**
G	7	13/14	93	4	8 **a**, 4 α, 1 α/**a**	**a**

Figure 5

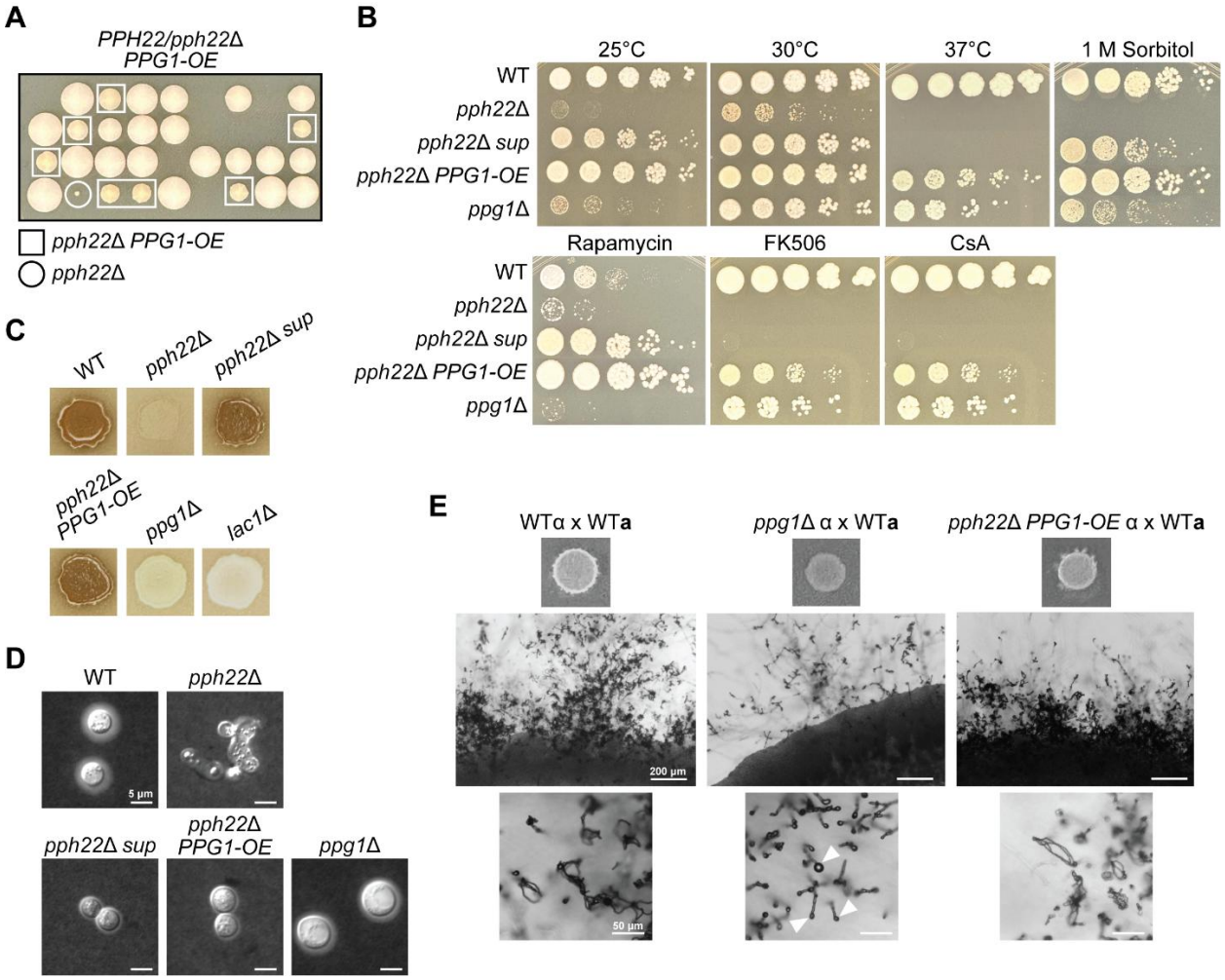
A
PPH22/pph22Δ
PPG1-OE
pph22Δ PPG1-OE
pph22Δ
B
25°C
30°C
37°C
1 M Sorbitol
WT
pph22Δ
pph22Δ sup
pph22Δ PPG1-OE
ppg1Δ
Rapamycin
FK506
CsA
C
WT
pph22Δ
pph22Δ sup
pph22Δ PPG1-OE
ppg1Δ
lac1Δ
D
WT
pph22Δ
5 µm
pph22Δ sup
pph22Δ PPG1-OE
ppg1Δ
E
WTα x WTa
ppg1Δ α x WTa
pph22Δ PPG1-OE α x WTa
200 µm
50 µm

Figure 6

A

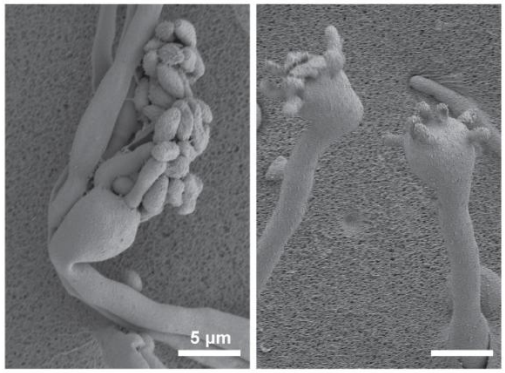

B

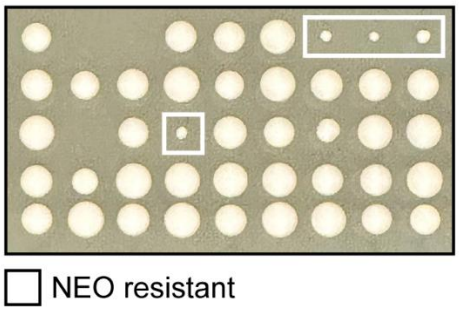

C

Spot	Basidia #	Spores germinated/ dissected	% Germination	NEO^R/ NAT^R	*MAT*	Mito.
far8Δ::NEO **a** (YSB11129) x H99α						
A	1	12/14	86	0	All α	**a**
	2	14/14	100	0	11 α, 3 α/**a**	**a**
B	3	13/20	65	12	5 **a**, 7 α, 1 α/**a**	**a**
C	4	3/5	60	2	1 **a**, 1 α, 1 α/**a**	**a**
	5	6/14	43	6	2 **a**, 1 α, 3 α/**a**	**a**
far8Δ::NEO **a** (YSB11132) x H99α						
D	1	12/13	92	0	All α	**a**
	2	8/13	62	0	All α	**a**
E	3	14/14	100	0	All α	**a**
	4	13/14	93	0	All α	**a**
F	5	9/14	64	0	All α	**a**
	6	18/18	100	0	All α	**a**
far8Δ::NAT α (YSB9100) x KN99**a**						
G	1	9/14	64	0	All **a**	**a**
	2	12/13	92	0	All **a**	**a**
H	3	12/14	86	0	All **a**	**a**
I	4	12/14	86	0	All **a**	**a**
	5	10/14	71	7	2 α, 8 α/**a**	**a**